Cold Regions Science and Technology 64 (2010) 174–181

Contents lists available at ScienceDirect

Cold Regions Science and Technology

journal homepage: www.elsevier.com/locate/coldregions

# In situ and photographic measurements of avalanche crown transects

Edward H. Bair [a,*], Karl W. Birkeland [b], Jeff Dozier [a]

[a] Bren School of Environmental Science & Management, University of California, Santa Barbara, CA, USA
[b] Forest Service National Avalanche Center, US Department of Agriculture, Bozeman, MT, USA

ARTICLE INFO

*Article history:*
Received 2 November 2009
Accepted 9 August 2010

*Keywords:*
Avalanche
Snow
Power law
Gaussian process

ABSTRACT

Despite its fundamental importance, crown depth is often treated as a scalar rather than a distributed variable in avalanche run-out and fracture models. To date, no studies have examined the distribution of depth across crown transects. We present results on geometry, depth distribution, and spatial correlation for transects along the crowns of small to large avalanches. Crown heights are fit well by normal or Weibull distributions and are spatially correlated. Transects are thinnest and decreasing toward the flanks, perhaps associated with fracture arrest. Underlying and adjacent terrain seems to have little influence on our transects. Instead, wind transported snow and upwind features play a dominant role. We suggest deposition of new snow by wind is a Gaussian process that drives transect shape. Comparing strength distributions and coefficients of variation from previous crown face studies, we suggest differences in overburden drive distributions of strength measured across crown faces.



## 1. Introduction

Detailed measurements of avalanche slabs are important for run-out models and fracture research. Because the avalanche destroys it, the slab is difficult to measure. A reasonable proxy is the crown face. After asserting that power laws in aggregate crown depth distributions may result from observers recording maximum depth (Bair et al., 2008), we decided to investigate parent distributions of these maxima by measuring depth transects across individual avalanche crown faces. Two researchers have noted slab taper (Perla, 1974, 1977; McClung, 2009), yet most studies treat slab depth as a scalar rather than a distributed variable. Both researchers comment on a lack of measurements across crown faces. Numerous studies find depth to the weak layer to vary spatially—see Schweizer et al. (2008) for reviews—so treatment of the slab as uniformly thick is inadequate. A few recent studies have used laser scanning and photogrammetry to construct snow-depth-difference maps before and after avalanches (Vallet et al., 2001; Sovilla et al., 2010), but none have reconstructed the slab. Slab depth has been called the "fundamental scaling parameter" (McClung, 2005), yet there are almost no field observations of its geometry for individual transects.

Conway and Abrahamson (1984) examine the stability index, defined as the ratio of shear fracture strength to overburden stress, across a 15 m wide crown face. They call low shear strengths under thin areas of the slab "deficit zones", and areas of high strength, "pinned zones". They attribute differences in shear strength to slab geometry formed by wind. Citing snow fence drift studies from Tabler (1980) and sand dune physics from Bagnold (1941), Conway and Abrahamson explain differences in slab geometry with longitudinal snow dunes, which have troughs and peaks in the lee direction, and also to traverse snow dunes, which have troughs and peaks normal to the wind direction.

Coarse slab depth measurements, taken plumb to the crown face, were published in Swiss avalanche accident reports prior to 1980. Some of these measurements were continued and used for stability index studies. Föhn (1988) measures the stability index across the crown of a large (180 m wide) avalanche. He reports similar findings as Conway and Abrahamson. Since the crown face he examines is triangular, with the center much further uphill than the flanks, Föhn finds deficit zones occur in bands. He attributes these bands to troughs of wind dunes that form in the down slope direction. Föhn does not consider the effect transverse dunes may have on slab geometry. He reports that slab depth is 30–40% lower in deficit zones and suggests shallow slab depths are associated with low shear and tensile strength.

The slab depth transects we were able to obtain from the Swiss accident collection ranged from 13–21 observations, at regularly and irregularly spaced intervals, for four avalanches ranging in depth from 5–185 cm. Because of the small sample size, we could not fit a distribution to these transects with any certainty. A study that uses photogrammetry (Vallet et al., 2001) reported just one crown depth transect. They did not find a tapering crown, nor was a statistical distribution fit to the depths. The avalanches they photographed were very large (ca. $10^5 m^3$), with crown depths ranging from 1.0 to 3.5 m. The measurements had an accuracy of $\pm 0.35$ m, which is not fine enough to capture a crown face that tapers to very small depths.

* Corresponding author.
*E-mail addresses:* nbair@bren.ucsb.edu (E.H. Bair), kbirkeland@fs.fed.us.gov (K.W. Birkeland), dozier@bren.ucsb.edu (J. Dozier).

0165-232X/$ – see front matter © 2010 Elsevier B.V. All rights reserved.
doi:10.1016/j.coldregions.2010.08.004

**Table 1**
Avalanches and normal distribution parameters.

| # | Location | Method | Width (m) | Max depth (cm) | Min depth (cm) | $\mu$ (cm) | $\sigma$ (cm) | $\frac{\sigma}{\mu}$ | Confined? | $N$ | $R^2$ normal | Class size |
|---|---|---|---|---|---|---|---|---|---|---|---|---|
| 1 | Paranoid 4, Mammoth, CA | *In situ* | 7 | 20 | 1 | 10 | 6 | 0.60 | Yes | 73 | 0.90 | R1 |
| 2 | Kayla's Brothers & The Right Stuff, Yellowstone Club, MT | *In situ* | 130 | 140 | 7 | 79 | 36 | 0.46 | Yes | 130 | 0.96 | R5 |
| 3 | Unknown, Columbia Mountains, BC | Photo | 149 | 100 | 28 | 70 | 14 | 0.20 | Yes | 168 | 0.97 | R3 |
| 4 | Unknown backcountry, CO | Photo | 42 | 72 | 7 | 39 | 17 | 0.44 | No | 81 | 0.96 | R3 |
| 5 | Crown Butte, Daisy Pass, Cooke City, MT | Photo | 84 | 63 | 20 | 44 | 9 | 0.20 | Yes | 88 | 0.99 | R3 |
| 6 | Dropout 1–3, Mammoth, CA | Photo | 100 | 213 | 29 | 129 | 30 | 0.23 | No | 87 | 0.92 | R3 |
| 7 | Climax, Mammoth, CA | Photo | 230 | 122 | 10 | 73 | 22 | 0.30 | No | 150 | 0.99 | R4 |
| 8 | Paranoid 4, Mammoth, CA | Photo | 69 | 200 | 24 | 98 | 46 | 0.47 | Yes | 111 | 0.97 | R4 |
| 9 | Dropout 1–3, Mammoth, CA | Photo | 100 | 655 | 148 | 446 | 147 | 0.33 | No | 80 | 0.91 | R5 |
| 10 | Dave's, Mammoth, CA | Photo | 385 | 457 | 42 | 288 | 90 | 0.31 | No | 77 | 0.96 | R5 |

Columns are (left to right): avalanche number, path name and area, method of measurement, measured geometry (width, max/min depth), normal distribution parameters ($\mu$ and $\sigma$), coefficient of variation ($\mu/\sigma$), whether or not the path is confined, sample size ($N$), normal correlation coefficient ($R^2$)–a measure of linearity on a normal probability plot, and size (1–5) relative to maximum (5).

We present the first study of detailed crown depth transect measurements. We hope these measurements will be useful for fracture research and will offer insight into triggering and avalanche formation.

## 2. Methods

Avalanches from four different states or provinces were measured (Table 1). We limit our examination to geometry and depth distributions of crown transects. We do not examine slab length, slab volume, or total avalanche volume because of the difficulty in measuring these variables. The crown is easier to measure both *in situ* and by photographic methods, since it is not partially or completed destroyed by the avalanche as are the flanks, stauchwall, and slab.

It is important to note that crown faces are also not uniform in their cross-slope geometry; most are convex, with an apex at varying uphill points to the start of the flanks (Perla, 1971). Also, slab taper has been observed both across the crown face and above it (Perla, 1974). Our two dimensional depth transects ignore these variations in uphill or downhill position of depth measurements. Further, many avalanches propagate across multiple aspects, bed surfaces, and slope angles.

### 2.1. In situ *methods*

During the winter of 2008–2009, we directly measured two crown line faces, one small and one large avalanche, both within one day of the avalanche (#1 and #2 in Fig. 1). The measurements were orthogonal to the bed surface and made at 0.10 and 1.00 m spacing, respectively. They covered the crown face from flank to flank, across the slope. The main source of error was finding the exact depth to the

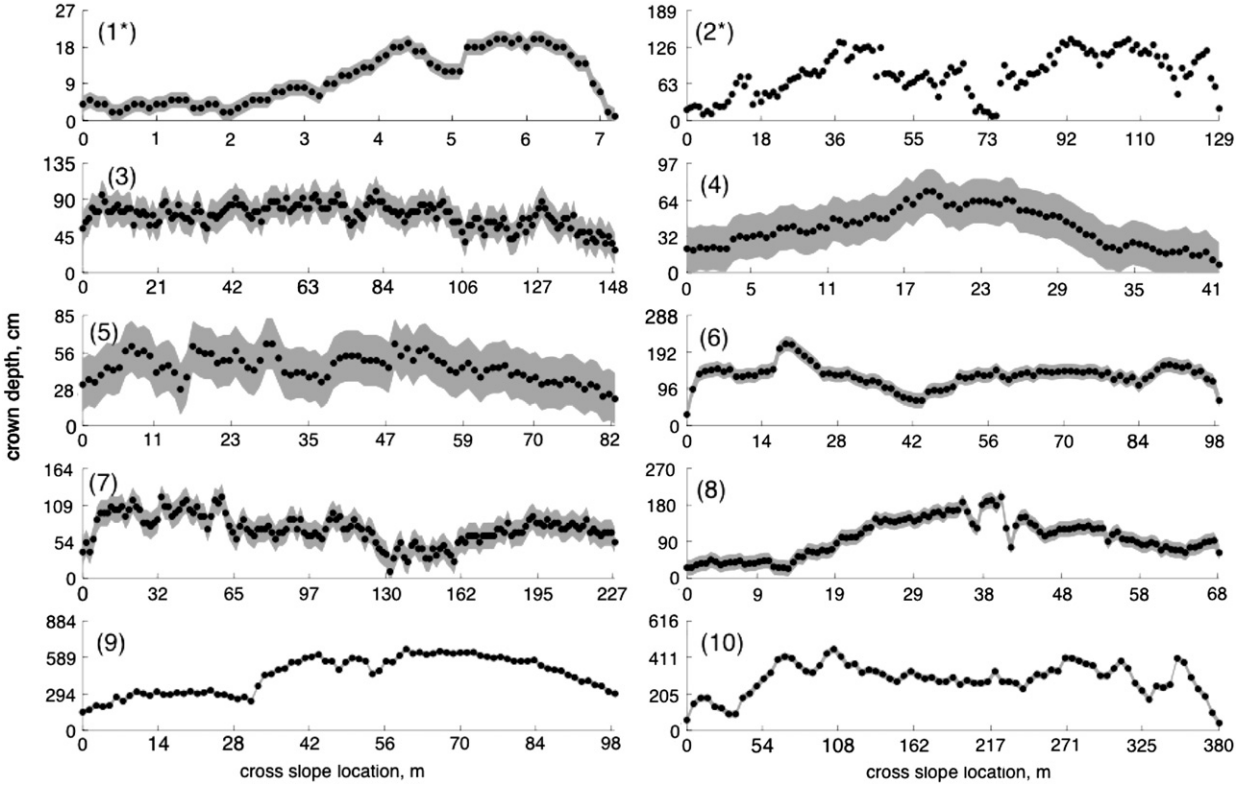


**Fig. 1.** Crown depth transects. Transects measured in situ (first two with stars), or photographically. The black dots are measured values, the gray shading is an error estimate: ± 2 cm for avalanches 1–2 and ± 20 cm for avalanches 3–10. The numeric labels correspond to avalanche numbers in Table 1.

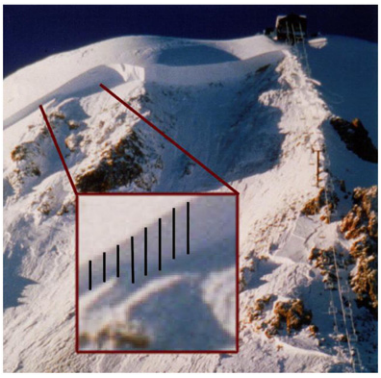

**Fig. 2.** Avalanche 9. Area near coordinate 3 m enlarged. The black lines show depths measured photographically. Photo courtesy of Mammoth Mountain Ski Patrol.

bed surface, especially after it was covered with wind-transported snow. Still, we believe the error was only 1–2 cm.

### 2.2. Two-dimensional photographic methods

We used 2-d photographic methods to measure transects for eight other avalanches (#3 through #10 in Fig. 1). Since crown faces are usually the most intact scar left by an avalanche, we are able to take advantage of digital photographs of them. We selected images where the crown face is oriented roughly orthogonally to the central line of sight and where lens distortion appears minimal.

Using a known length of some reference object in the photograph, such as a person or a measured maximum crown depth, we scale our measurements. The enlarged area in Fig. 2 shows an example of photographic measurements, taken for avalanche 9. Photographic methods are less accurate than in situ measurements. Sources of error include image resolution, distortion, look angle, reference object uncertainty, and distinguishing the bed surface. We estimate the error to be at least the resolution of the image, about 10–20 cm. Keeping these limitations in mind, we find photographic methods essential for increasing our sample size, which is otherwise restricted by the labor required to directly measure the distribution of sizes along the crown.

Photographic methods are especially useful for examining general geometry, spatial correlation, and comparing transects. Given that we are only making 2-d, rather than 3-d measurements, we can avoid using fixed control points, stereo plotters, and other photogrammetric tools.

### 2.3. Statistical distributions of crown depths

We fit nine candidate statistical distributions using maximum likelihood. The distributions fit were the: exponential, normal, Fréchet, Weibull, generalized extreme value, truncated power law, lognormal, uniform, Cauchy, and Gumbel (Table 2). We select distributions by comparing squared correlation coefficients, $R^2$, for linear regressions on probability plots (Chambers et al., 1983), as Table 2 shows.

### 2.4. Autocorrelation using correlation coefficients

We computed unbiased correlation coefficients at all lags using standard signal processing software (Orfanidis, 1996; MathWorks, 2009). We then normalized on a 0 to 1 scale by dividing each coefficient by the maximum computed raw coefficient. The result is a vector of correlation coefficients, $R$, which measure autocorrelation as a function of lag.

### 2.5. Influence of underlying terrain

We examine the influence of underlying topography for transects from Mammoth Mountain (avalanches 1 & 6–10) using a high-resolution (1 $m^2$) digital elevation model (DEM). By drawing transects that follow our crown transects, we calculate transects of the underlying topography.

## 3. Results

### 3.1. Geometry

Depths range over three orders of magnitude. Transects generally are thinner and decrease in depth toward the flanks (Fig. 1). For instance, avalanches 1 and 2, which have the lowest estimated error since they were measured by hand, have depths at the flanks of 10–40% of their mean crown depth. Avalanches 3–10 have depths at the flanks of 18–77% of their mean crown depth (Fig. 1 and Table 1). Based on others' observations (Perla, 1977; McClung, 2009), we might

**Table 2**
Distributions, average $R^2$, and parameters.

| Name | Probability density function (pdf) with 1,2, or 3 parameters | $\overline{R}^2$ | 1st parameter range | | 2nd parameter range | | 3rd parameter range | |
|---|---|---|---|---|---|---|---|---|
| Exponential | $pdf(x\|\mu)=\mu\exp(-\mu x)$ | 0.74 | 10 | 446 | | | | |
| Normal | $pdf(x\|\mu,\sigma)=\frac{1}{\sqrt{2\pi^2}}\exp\left(-\frac{(x-\mu)^2}{2\sigma^2}\right)$ | 0.95 | 10 | 446 | 6 | 148 | | |
| Fréchet | $pdf(x\|\alpha,\sigma)=\alpha\exp\left(-\left[\frac{x}{\sigma}\right]^{-\alpha}\right)\left(\frac{x}{\alpha}\right)^{-1-\alpha}$ | 0.43 | 1.20 | 3.65 | 5 | 342 | | |
| Weibull | $pdf(x\|\beta,\eta)=\eta\beta^{-\eta}x^{\eta-1}\exp\left(-\left[\frac{x}{\beta}\right]^{\eta}\right)$ | 0.95 | −6.02 | −1.64 | 11 | 498 | | |
| Generalized extreme value | $pdf(x\|\xi,\mu,\sigma)=\frac{1}{\sigma}\left(1+\xi\left[\frac{x-\mu}{\sigma}\right]\right)^{\frac{-1}{\xi-1}}\exp\left(-1+\xi\left[\frac{x-\mu}{\sigma}\right]-\frac{1}{\xi}\right)$ | 0.96 | −0.74 | −0.08 | 5 | 169 | 7 | 427 |
| Truncated power law | $pdf(x\|\alpha,x_{\min})=-(1+\alpha)x_{\min}^{-(1+\alpha)}$, where $x_{min}$ is the minimum cutoff for the power law (Clauset et al., 2007) | 0.58 | 1.79 | 15.20 | 3 | 550 | | |
| Lognormal | $pdf(x\|\mu,\sigma)=\frac{1}{x\sigma\sqrt{2\pi}}\exp\left(-\frac{(\ln x-\mu)^2}{2\sigma^2}\right)$ | 0.83 | 2 | 6 | 0.23 | 0.77 | | |
| Uniform | $pdf(x\|N)=\frac{1}{N}$,where $N$ is the number of depths measured | 0.95 | 73 | 168 | | | | |
| Cauchy | $pdf(x\|\mu,\sigma)=\frac{\sigma}{\pi(\sigma^2+\|x-\mu\|^2)}$ | 0.35 | 8 | 499 | 5 | 109 | | |
| Gumbel | $pdf(x\|\mu,\sigma)=\frac{\left[\exp\left(-\left[\frac{x-\mu}{\sigma}\right]\right)\exp\left(-\exp\left(-\left[\frac{x-\mu}{\sigma}\right]\right)\right)\right]}{\sigma}$ | 0.87 | 5 | 140 | 7 | 371 | | |

Columns are (left to right): distribution name, function, average correlation coefficient $\left(\overline{R}^2\right)$–a measure of average linearity on a probability plot for all 10 avalanches, and ranges for parameters, listed left to right, in the *pdf*.

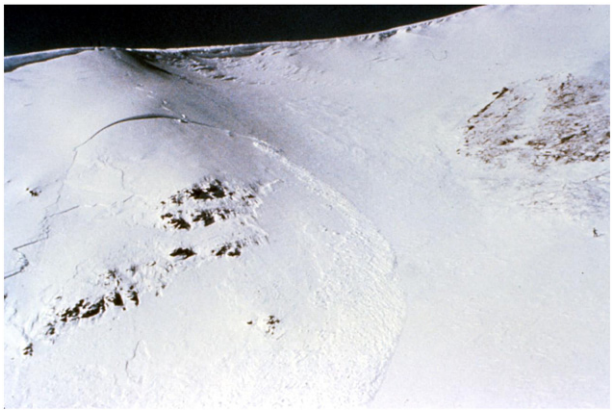

**Fig. 3.** Avalanche 4. Crown taper on an atypical path with a cross-slope convexity. Photo courtesy of the National Avalanche Center.

expect that confined paths, such as those abutted by rock walls or dense trees, show more tapering than unconfined paths. Jamieson and Johnston (1992) were among the first to define unconfined paths as those that do not taper to less than half the mean crown thickness and do not abut rock walls or dense timber. Some of our transects contain one criterion, by this definition, but not the second. For instance, our measurements show a smooth taper towards the flanks in some fractures (1, 4, 8, & 9) but not in others, regardless of whether the path is abutted by rock walls or timber. Consider the photographs and transects for avalanches 4 and 5. The transect for avalanche 4 shows smooth tapering on both sides (Fig. 1). It is not abutted by trees or rock outcroppings on either side (Fig. 3). The transect for avalanche 5 does not show tapering, the first criterion of confinement, although it is generally thinner at the flanks (Fig. 1). There are rock outcroppings to the left and right of the main area of the fracture, showing that this fracture may have been arrested by the terrain (Fig. 4). This example shows that rock walls on the sides of a path do not necessarily play a role in crown taper.

**Fig. 4.** Avalanche 5. A crown that does not taper, despite terrain barriers. Photo courtesy of the Gallatin National Forest Avalanche Center.

In avalanche 7 (Fig. 5a), moguls are visible above the crown, which may cause the rough sinusoidal noise present throughout the transect. In avalanche 10 (Fig. 5b), rain runnels caused by a rain on snow event show up clearly as local minima at 40, 90, 300, and 325 m.

### 3.2. Depth distributions

The normal (Fig. 6), uniform, Weibull, and generalized extreme value distributions had the highest average $R^2$ values, 0.95–0.96 (Table 2), so any of these distributions models transect depths adequately. The normal distribution is the parsimonious choice over the generalized extreme value, given that it has two parameters instead of three. The generalized extreme value likely overfits, as adding an extra parameter only yields a 0.01 increase in the average $R^2$ value. The uniform distribution, most often used in random number generators, gives the same average $R^2$ (0.95) as the normal.

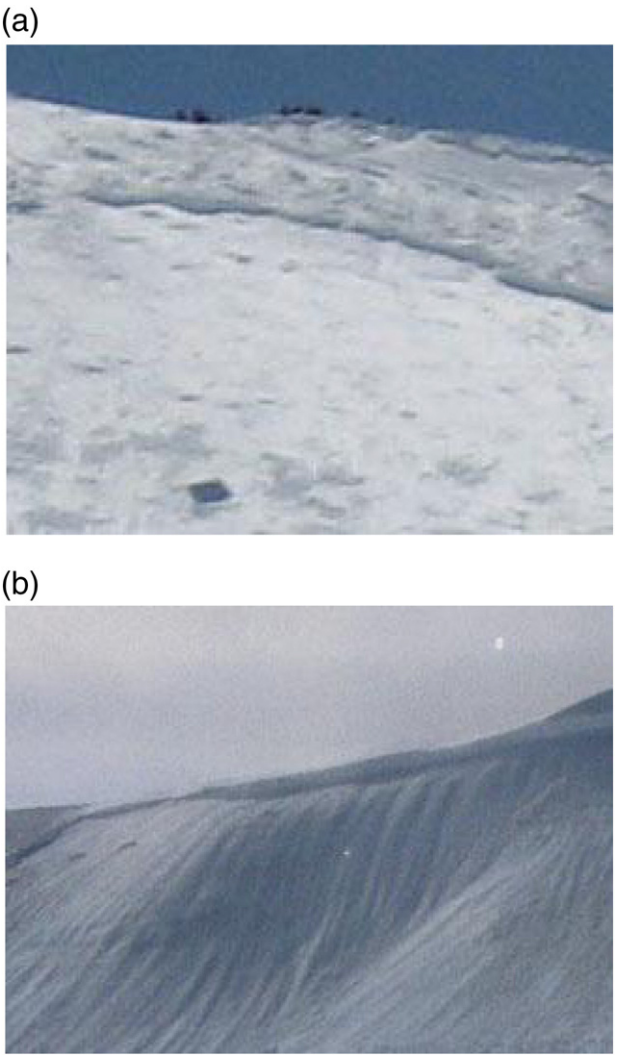


**Fig. 5.** a and b. Close up view of avalanches 7 and 10. Image (a) shows moguls above the crown. Images (b) shows rain runnels on the bed surface. Photos courtesy of Mammoth Mountain Ski Patrol.

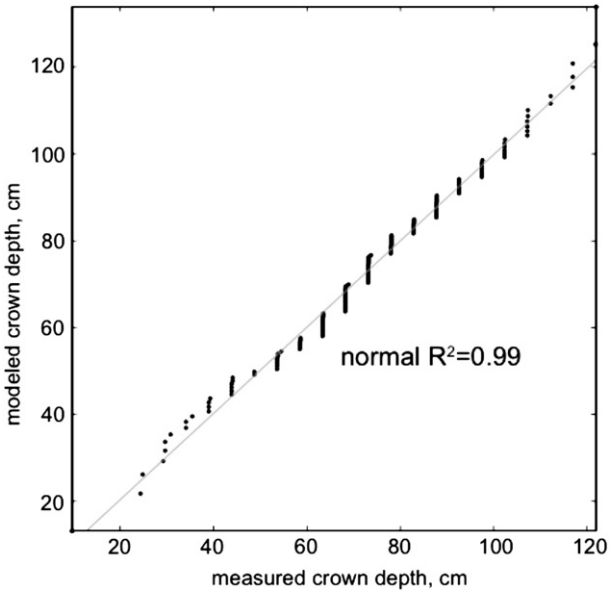


**Fig. 6.** Normal probability plot for avalanche 7. The horizontal axis shows measured depths and the vertical axis shows crown depths modeled with a normal distribution using parameters $\mu = 73$ cm and $\sigma = 22$ cm.

Lastly, the Weibull and the normal, both two-parameter distributions, fit the transects equally well, which is to be expected, since a Weibull distribution can often be used interchangeably with a normal given the right shape parameter, $\eta$ (Table 2). The Weibull has the advantage of being positive for all parameter values, whereas the normal has negative values, which cannot occur in real transects. Conversely, the parameters of the normal are easier to interpret. Using normal distributions, the coefficients of variation in depth, $CV = \sigma/\mu$, range from 20 to 60% with an average value of 35% (Table 1).

### 3.3. Autocorrelation

Crown transects have strong spatial correlation. A vector of correlation coefficients, $R$, is greater than 0.5 up to lags of approximately half the transect width (Fig. 7).

### 3.4. Underlying terrain

The underlying terrain transects are smooth (Fig. 8) and normally distributed (Table 3). This is not surprising given that most starting zones are located on smooth pumice slopes (Mammoth Mountain is a young lava dome). The most important feature of the terrain transects is that they do not resemble their corresponding crown transects (Fig. 1). We find that underlying terrain that becomes deeply buried has little effect on crown face geometry.

## 4. Discussion

### 4.1. Geometry

No crown transects have uniform depth values, because wind loading causes differences in slab geometry. Variation in overburden may explain strength variation across crown faces reported in previous studies (Perla, 1977; Conway and Abrahamson, 1984; 1988; Föhn, 1988). As with our transect depths, normal distributions have been used to model shear strengths across crown lines (Perla, 1977; Sommerfeld and King, 1979). Our average CV of 35% is close to the strength CV values reported in the above studies and 2–3× greater than the CV in snow depth for a 18 m × 45 m wind sheltered study site (Birkeland et al., 1995). For instance, in 28 measurements at the bed surface of a crown face, Perla (1977) reports a mean value of 493 Pa, with a standard deviation of 142 Pa, giving a CV of 29%. The stability index across a crown face shows similar variability. Föhn (1988) shows a CV of 33% for 44 stability index measurements across a 170 m crown face.

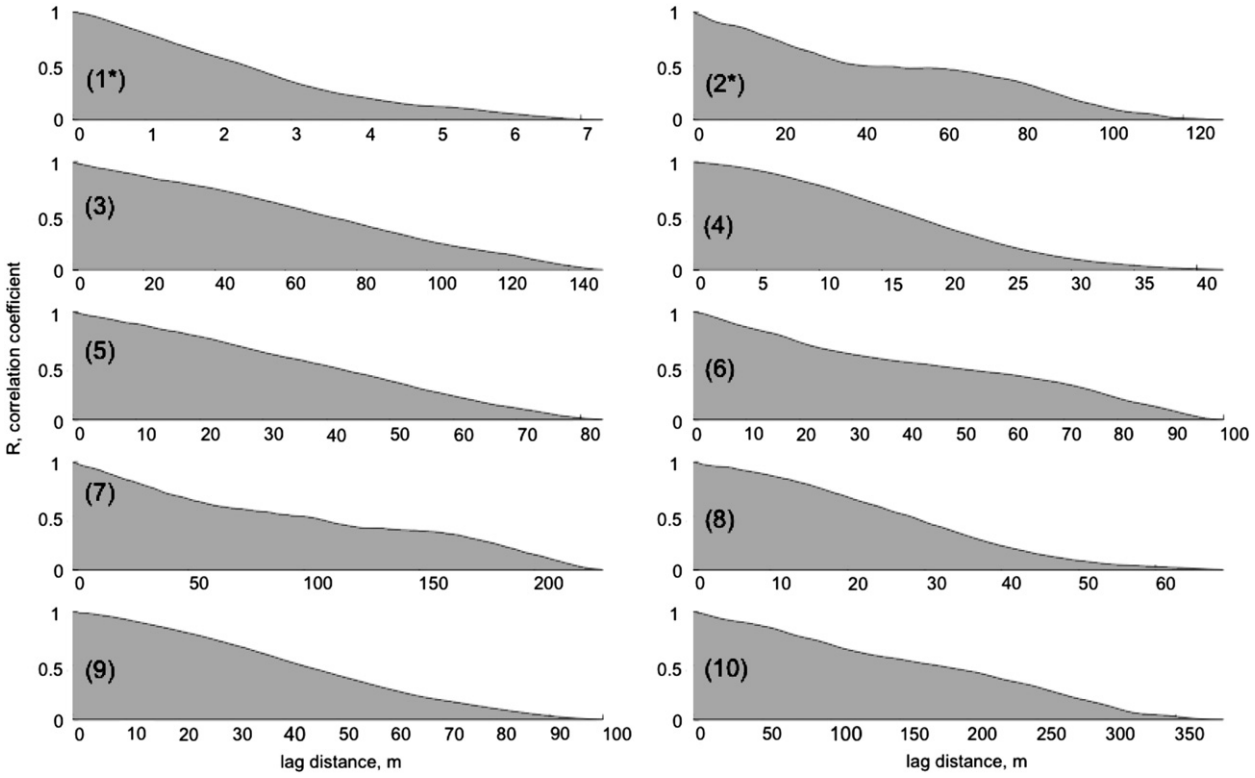


**Fig. 7.** Correlation coefficients. The horizontal axis shows distance lag, in meters, and the vertical axis shows the correlation coefficient $R$.

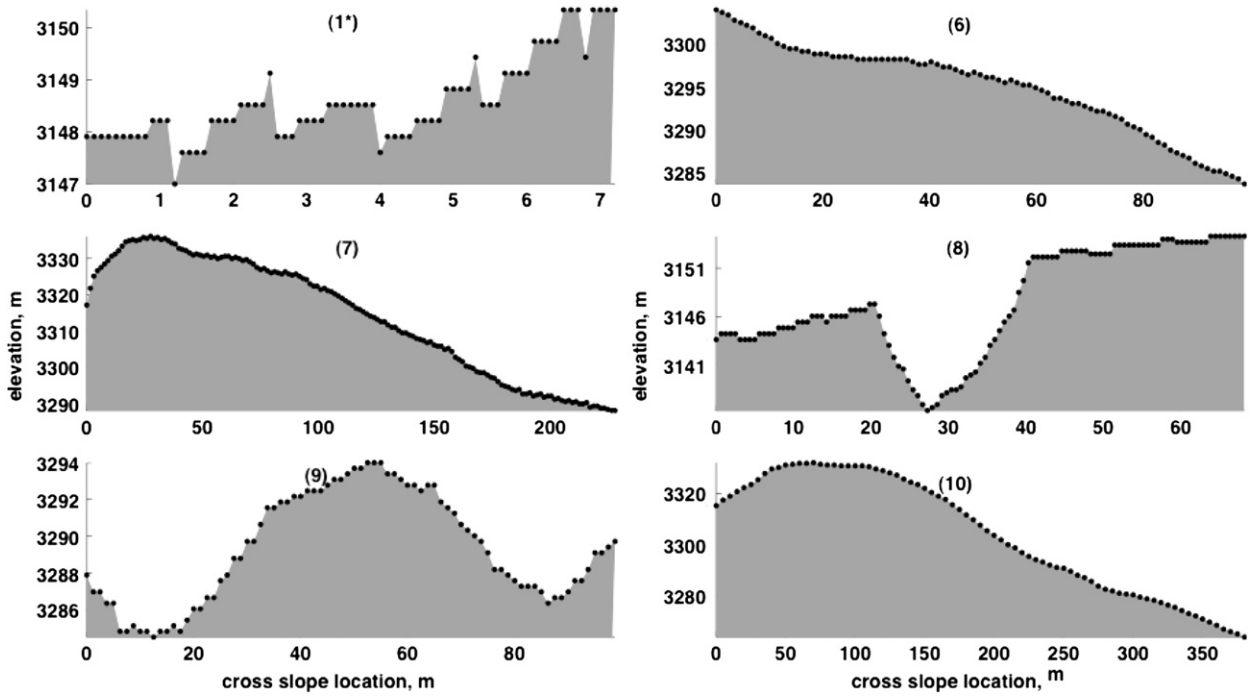


**Fig. 8.** Underling terrain transects for avalanches 1 and 6–10. The vertical axes are elevations and the horizontal axes are cross slope locations corresponding to locations in Fig. 1.

Föhn's (1988) and Conway and Abrahamson's (1984) findings that thin slab depths are associated with deficit zones can be explained by a lack of strength due to compaction from overburden. Strengthening in response to snowfall has been documented for various types of snow: new snow (Roch, 1966), large rounded grains (Roch, 1966), surface hoar (Zeidler and Jamieson, 2006b), and faceted crystals (Zeidler and Jamieson, 2006a; Jamieson et al., 2007). The mechanisms by which snow densifies and strengthens include sintering and compaction; denser snow has greater strength, but the relationship has considerable scatter so some other snow property also affects strength (Keeler and Weeks, 1968; Mellor, 1974; Perla, 1974; Jamieson, 1995).

Whether snow strengthens and does not avalanche, or reaches the critical stress and strain rates and fails, depends on loading rate. Rapid loading ($\geq$2.5 cm h$^{-1}$) causes instability (Schweizer et al., 2003), since overburden shear stress often exceeds fracture strength. In this case, the stability index declines toward 1, and natural avalanching occurs. Rapid wind loading, combined with a ski or explosive trigger, is the main cause of failure for the Mammoth transects (1 & 6–10), where > 90% of avalanches occur within the new snow layer or at interface between the new and old snow. Conversely, slower loading increases shear strength.

Moreover, crown and slab geometry may affect fracture propagation. The preponderance of thin depths at the flanks suggests that thinning is associated with fracture arrest. Other avalanche fracture research finds that slab thickness is an important parameter in fracture propagation (McClung, 1981; Jamieson and Johnston, 1992; Bažant et al., 2003; Schweizer et al., 2003; McClung, 2005; McClung and Schweizer, 2006; Heierli et al., 2008). Jamieson and Johnston (1992) derive an arrest parameter for slab width $W$ which is proportional to the square of the slab depth, $D$:

$$W \propto \left(\frac{D\gamma}{\tau}\right)^2 \quad (1)$$

where $\gamma$ is slab tensile strength and $\tau$ is basal shear strength.

Over two winters, Simenhois and Birkeland (2008) studied fracture propagation in 52 snow pits in Colorado and New Zealand using extended column and propagation saw tests. In side-by-side tests comparing fractures initiated at thick sections of slabs next to fractures initiated at thin sections of slabs, they found that weak layers fractured consistently from thin to thick sections, but fractures arrested in the other direction. They note that slabs often fractured perpendicularly to the weak layer before the crack reached the other end of the slab, when traveling from thick to thin sections. They suggest that once under a thin section, the fracture may turn perpendicularly to the shear and form a tensile fracture. Fracture arrest in snow is not well understood and does not explain findings by Simenhois and Birkeland (2008). All other factors being equal, we suggest that thin areas of the slab are weaker and fracture more easily than thick areas. For this reason, fractures perpendicular to the shear plane form in thin areas. This may explain why we find shallow transect depths at the flanks.

**Table 3**
Underlying terrain transects and normal distribution parameters.

| Avalanche # | $\mu$ (m) | $\sigma$ (m) | $R^2$ normal |
|---|---|---|---|
| 1 | 3149 | 1 | 0.88 |
| 2 | 3295 | 5 | 0.95 |
| 3 | 3314 | 16 | 0.90 |
| 4 | 3147 | 6 | 0.90 |
| 5 | 3289 | 3 | 0.93 |
| 6 | 3304 | 23 | 0.90 |

Underlying terrain for avalanches 1 and 6–10. Columns are: avalanche number (see Table 1), elevation mean ($\mu$) and standard deviation ($\sigma$) in meters, and normal correlation coefficient ($R^2$ normal).

### 4.2. Influence of upwind features

Our explanation for crown shape agrees with Conway and Abrahamson (1984) and Föhn (1988): upwind terrain features and their interaction with the wind dominate transect shape. We attribute the wave patterns in transects to snow dunes in lee and normal directions to the wind. Tabler (1980) has conducted extensive measurements of snow dunes behind wind fences. He finds that maximum depth, length, and cross-sectional (lee directional area of

snow dunes scale with snow fence height. Tabler also explains why we see convex shapes in some transects. Lee drifts in transects parallel to fences are convex because of turbulence generated at the edges of wind fences. Turbulence causes winds to accelerate and sweep around the edges, stripping snow at fence edges of drifts.

High wind speeds also cause significant density increases through compaction. For horizontal slat fences, Tabler (1980) fits a power law that scales mean density with fence height to over 1000 density measurements spanning 16 years. The increased overburden and density in lee snow dunes may form what Conway and Abrahamson (1984) call pinned zones, while shallow wind stripped zones remain uncompacted and might form so-called deficit zones.

### 4.3. Statistical distributions

None of the transects is fit by heavy-tailed distributions such as the Fréchet or power law. Bair et al. (2008) show that the maximum crown depths of more than 64,000 avalanches have power law distributions. Recording only the maximum crown depth for each avalanche, a commonly observed practice for avalanche workers, can lead to power law distributed aggregates. Crown depth aggregates belong to the Fréchet maximum domain of attraction, which suggests parent distributions (individual avalanche crown depths) will also be heavy-tailed.

How can we reconcile the fact that our transects are normally distributed and not heavy-tailed? Distributions of aggregates involve large scales which depend on how the data are grouped. For instance, in Bair et al. (2008) we examined 39 seasons of crown depths at the path and ski area scale. For single avalanche crown transects, the relevant scales are much smaller; they involve slope-scale processes such as wind redistribution, underlying snow cover, and terrain. The large difference in scales between aggregate and transect distributions make comparison of generating mechanisms difficult.

We suggest individual transects are driven by spatial distributions of new snow. Normal distributions result from a Gaussian process (Cressie, 1993), where measurements are spatially correlated. A Gaussian process (GP) is "a collection of random variables, any finite number of which have a joint Gaussian distribution" (Rasmussen and Williams, 2006). Spatial interpolation (e.g. kriging) with a Gaussian prior distribution is an example of a GP. GPs have been used to interpolate snow depths in avalanche terrain. Chernouss and Fedorenko (1998) use a Gaussian process with an empirically derived covariance function to model snow depth for a single avalanche starting zone. Seidou et al. (2006) used GPs to interpolate SWE in the Gatineau basin of Quebec, Canada. They found GPs offered more information on the spatial distribution of SWE compared with ordinary kriging. Wind transport of snow smoothes surfaces by filling depressions and scouring ridges (Elder et al., 1991; Winstral et al., 2002); therefore it is natural to consider it as a spatially correlated Gaussian process.

## 5. Conclusion

We examined the geometry, distribution, spatial correlation, and underlying terrain of 10 avalanche crown depth transects. We find non-uniform spatially correlated transect depths, best fit by normal and Weibull distributions. We suggest normally distributed transects result from a spatially correlated Gaussian process, i.e. new snow deposition, with wind loading being the primary driver of the transect geometry. This leads to differences in strength and stress within the slab, which can be summarized by a stability index. Normally distributed shear strengths across crown faces, with similar CVs to our measured crown depths, indicate that slab depth and its effect on compaction might be responsible for shear strength distributions measured across crown faces in prior studies.

Transects do not have power law tails. The gap between normal transects and power law aggregates (Bair et al., 2008) results from the different scales involved. Aggregate distributions are driven by large scale processes, while transects are driven by slope-scale processes.

Though we know of no detailed 3-d reconstructions of slab depth in the literature, our results suggest that depth in such reconstructions would be spatially correlated and bivariate normally distributed, with noticeable tapering at the flanks. A recommendation for future work is to use a combination of terrestrial laser scanning and synthetic aperture radar to measure distribution of snow depth in avalanche starting zones (Schaffhauser et al., 2008).

## Acknowledgements

We thank Ron Simenhois, Doug Catherine, Christine Pielmeier, Roland Meister, and those who contributed images. We also thank Juerg Schweizer and the anonymous reviewers for their comments, especially one reviewer's comments on Gaussian processes. This research was funded by NSF Grant EAR-0537327. The first author is supported by a student fellowship from the U.S. Army Cold Regions Research and Engineering Laboratory.

## References

Bagnold, R.A., 1941. The physics of blown sand and desert dunes. Methuen, London. 320 pp.
Bair, E.H., Dozier, J., Birkeland, K.W., 2008. Avalanche crown-depth distributions. Geophysical Research Letters 35, L23502. doi:10.1029/2008GL035788.
Bažant, Z.P., Zi, G., McClung, D., 2003. Size effect law and fracture mechanics of the triggering of dry snow slab avalanches. Journal of Geophysical Research 108, 2119. doi:10.1029/2002JB001884.
Birkeland, K.W., Hansen, K.J., Brown, R.L., 1995. The spatial variability of snow resistance on potential avalanche slopes. Journal of Glaciology 41, 183–190.
Chambers, J., Cleveland, W., Kleiner, B., Tukey, P., 1983. Graphical methods for data analysis. Wadsworth, Belmont, CA. 336 pp.
Chernouss, P.A., Fedorenko, Y.K., 1998. Probabilistic evaluation of snow-slab stability on mountain slopes. Annals of Glaciology 26, 303–306.
Clauset, A., Shalizi, C.R., Newman, M.E.J., 2007. Power-law distributions in empirical data. arXiv: 0706.1062v1.
Conway, H., Abrahamson, J., 1984. Snow stability index. Journal of Glaciology 30, 321–327.
Conway, H., Abrahamson, J., 1988. Snow slope-stability: a probablistic approach. Journal of Glaciology 34, 170–177.
Cressie, N.A.C., 1993. Statistics for spatial data. Wiley-Interscience, New York. 928 pp.
Elder, K., Dozier, J., Michaelsen, J., 1991. Snow accumulation and distribution in an alpine watershed. Water Resources Research 27, 1541–1552. doi:10.1029/91WR00506.
Föhn, P.M.B., 1988. Snowcover stability tests and the areal variability of snow strength. Proc. 1988 Intl. Snow Sci. Workshop, Whistler, B.C. Canada, pp. 262–273.
Heierli, J., Gumbsch, P., Zaiser, M., 2008. Anticrack nucleation as triggering mechanism for snow slab avalanches. Science 321, 240–243. doi:10.1126/science.1153948.
Jamieson, J. B. (1995), Avalanche prediction for persistent snow slabs, PhD Thesis, University of Calgary, Calgary AB, Canada, 258 pp.
Jamieson, J.B., Johnston, C.D., 1992. A fracture-arrest model for unconfined dry slab avalanches. Canadian Geotechnical Journal 29, 61–66. doi:10.1139/t92-007.
Jamieson, B., Zeidler, A., Brown, C., 2007. Explanation and limitations of study plot stability indices for forecasting dry snow slab avalanches in surrounding terrain. Cold Regions Science and Technology 50, 23–34. doi:10.1016/j.coldregions.2007.02.010.
Keeler, C.M., Weeks, W.F., 1968. Investigations into the mechanical properties of alpine snow-packs. Journal of Glaciology 7, 243–271.
MathWorks, 2009. MATLAB Signal Processing Toolbox 6.12: User's Guide. The MathWorks, Natick, MA. 1561 pp.
McClung, D.M., 1981. Fracture mechanical models of dry slab avalanche release. Journal of Geophysical Research 86, 10783–10790. doi:10.1029/JB086iB11p10783.
McClung, D.M., 2005. Dry slab avalanche shear fracture properties from field measurements. Journal of Geophysical Research 110, F04005. doi:10.1029/2005JF000291.
McClung, D.M., 2009. Dimensions of dry snow slab avalanches from field measurements. Journal of Geophysical Research 114, F01006. doi:10.1029/2007JF000941.
McClung, D.M., Schweizer, J., 2006. Fracture toughness of dry snow slab avalanches from field measurements. Journal of Geophysical Research 111, F04008. doi:10.1029/2005JF000403.
Mellor, M., 1974. A review of basic snow mechanics. In: LaChapelle, E.R., Kuroiwa, D., Salm, B. (Eds.), Snow Mechanics Symposium, 114. IAHS Publication, Wallingford, UK, pp. 251–291.
Orfanidis, S.J., 1996. Optimum signal processing: an introduction, 2nd ed. Prentice-Hall, Englewood Cliffs, NJ. 590 pp.
Perla, R. I. (1971), The slab avalanche, PhD Thesis, Department of Meteorology, University of Utah, Salt Lake City, UT.
Perla, R.I., 1974. Stress and fracture of snow slabs. In: LaChapelle, E.R., Kuroiwa, D., Salm, B. (Eds.), Snow Mechanics Symposium, 114. IAHS Publication, Wallingford, UK, pp. 208–221.

Perla, R., 1977. Slab avalanche measurements. Canadian Geotechnical Journal 14, 206–213. doi:10.1139/t77-021.
Rasmussen, C.E., Williams, C.K.I., 2006. Gaussian processes for machine learning. MIT Press, Cambridge. 266 pp.
Roch, A., 1966. Les variations de la resistance de la neige. In: de Quervain, M.R. (Ed.), Scientific Aspects of Snow and Ice Avalanches, 69. IAHS Publication, Gentbrugge, Belgium, pp. 182–195.
Schaffhauser, A., Adams, M., Fromm, R., Jörg, P., Luzi, G., Noferini, L., Sailer, R., 2008. Remote sensing based retrieval of snow cover properties. Cold Regions Science and Technology 54, 164–175. doi:10.1016/j.coldregions.2008.07.007.
Schweizer, J., Jamieson, B., Schneebeli, M., 2003. Snow avalanche formation. Reviews of Geophysics 41, 1016. doi:10.1029/2002RG000123.
Schweizer, J., Kronholm, K., Jamieson, J.B., Birkeland, K.W., 2008. Review of spatial variability of snowpack properties and its importance for avalanche formation. Cold Regions Science and Technology 51, 253–272. doi:10.1016/j.coldregions.2007.04.009.
Seidou, O., Fortin, V., St-Hilaire, A., Favre, A.-C., El Adlouni, S., Bobée, B., 2006. Estimating the snow water equivalent on the Gatineau catchment using hierarchical Bayesian modelling. Hydrological Processes 20, 839–855. doi:10.1002/hyp. 6127.
Simenhois, R., Birkeland, K.W., 2008. The effect of changing slab thickness on fracture propagation. Proc. 2008 Intl. Snow Sci. Workshop, Whistler, BC, Canada.
Sommerfeld, R.A., King, R.M., 1979. A recommendation for the application of the Roch index for slab avalanche release. Journal of Glaciology 22, 547–549.
Sovilla, B., McElwaine, J., Schaer, M., Vallet, J., 2010. Variation of deposition depth with slope angle in snow avalanches: measurements from Vallée de la Sionne. Journal of Geophysical Research 115, F02016. doi:10.1029/2009JF001390.
Tabler, R.D., 1980. Geometry and density of drifts formed by snow fences. Journal of Glaciology 26, 405–419.
Vallet, J., Gruber, U., Dufour, F., 2001. Photogrammetric avalanche volume measurements at Vallée de la Sionne. Switzerland, Annals of Glaciology 32, 141–146.
Winstral, A., Elder, K., Davis, R.E., 2002. Spatial snow modeling of wind-redistributed snow using terrain-based parameters. Journal of Hydrometeorology 3, 524–538. doi:10.1175/1525-7541(2002) 003<0524:SSMOWR>2.0.CO;2.
Zeidler, A., Jamieson, B., 2006a. Refinements of empirical models to forecast the shear strength of persistent weak layers. Part A: Layers of faceted crystals. Cold Regions Science and Technology 44, 194–205. doi:10.1016/j.coldregions.2005.11.005.
Zeidler, A., Jamieson, B., 2006b. Refinements of empirical models to forecast the shear strength of persistent weak layers. Part B: Layers of surface hoar crystals. Cold Regions Science and Technology 44, 184–193. doi:10.1016/j.coldregions.2005.11.004.